The Effects of Mg Microaddition on the Mechanical Behavior and Fracture Mechanism of MAR-M247 Superalloy At Elevated Temperatures

H.Y. BOR, C.G. CHAO, and C.Y. MA

The effects of microadditions of Mg on the mechanical behavior and fracture mechanism of MAR-M247 superalloy were investigated in this study. The microstructural observations and image analysis showed that a Mg microaddition ranging from 30 to 80 ppm significantly changed the primary MC carbide characteristics and inhibited the scriptlike carbide formation. After a 80 ppm Mg addition, the elongation measured at 1172 K increased over 3 times found that for the Mg-free MAR-M247 superalloy. The creep life and rupture elongation of the MAR-M247 superalloy with 80 ppm Mg was also improved up to 3 to 5 times that of the alloy without Mg during a 1033 K/724 MPa creep test. The fracture analyses demonstrated that cracks were mainly initiated and propagated at the interface of scriptlike MC carbides in the Mg-free MAR-M247 superalloy at elevated temperatures. The Mg microaddition effectively refined and spheroidized these coarse carbides so that a change in the crack initiation occurred from the carbide/matrix interface to that along the γ-γ' eutectic. Interfacial analysis using Auger electron spectroscopy illustrated that Mg segregated to the interface of the MC carbide/matrix, causing a change in the morphology and interfacial behavior of the carbides. This improvement contributed to a prolonged rupture life and upgraded the moderate temperature ductility of the MAR-M247 superalloy.

I. INTRODUCTION

DUE to optimal alloy design and microstructural modification, the MAR-M247* superalloy exhibits a variety of excellent characteristics, including good castability, good strength levels, superior creep, and hot corrosion resistance at elevated temperatures.[1–4] During the past 2 decades, this alloy has been widely employed in fabricating advanced turbine blades and rotating parts in the aerospace industry. However, from previous studies,[5,6] MAR-M247 has a drawback in that it exhibits low ductility under creep conditions of moderate temperature and high stress. This drawback might be related to grain boundary intrinsic behavior, coarse carbides, or some deleterious factors such as harmful phases and defects. In particular, the carbide characteristics can play a crucial role in determining the high-temperature properties of the MAR-M247 superalloy.[6]

The behavior of a carbide in superalloys is complex. In general, discrete carbides precipitating at grain boundaries (GBs) can inhibit GB sliding to improve the strength and creep behavior of superalloys at elevated temperatures. Conversely, the coarse or scriptlike MC primary carbides that exist within the grain interior or at GB are regarded as the factor leading to low ductility during creep and tensile tests.[7,8] Because of the extremely brittle property of MC carbides, they may act as crack initiation sites and propagation paths.[6,9] In order to minimize these detrimental effects, refinement and modification of coarse MC carbides through processing or microalloying are thought to be desirable and effective.

In recent investigations,[10–14] it has been shown that microadditions of Mg or Ca significantly enhance rupture life, ductility, and hot workability at elevated temperatures in some wrought superalloys. Particularly, the Mg microaddition has been shown to improve the impact toughness, hot workability, creep life, and ductility in several wrought superalloys.[15–27] These improvements are mainly attributed to the refinement of GB carbides arising from the segregation of Mg to the GB or to the carbide/matrix interface.[28–32] It is also proposed that carbide refinement may be associated with a decrease in carbide/matrix interfacial energy or the inhibition of coarse carbide growth.[33–36] However, little work has been reported on introducing Mg as a microalloying element in cast superalloys, which are generally poor in ductility and toughness at room and elevated temperatures. This property is essential both from the viewpoint of manufacturing concerns and service requirements where the rupture ductility is of importance. In this study, the effects of Mg microadditions on the mechanical behavior of MAR-M247 superalloy, in particular on the moderate temperature creep properties and fracture mechanism, are investigated in detailed. The objectives are to determine the fracture mode arising from Mg incorporation in the MAR-M247 superalloy and to analyze the possible mechanisms responsible for the improvement of moderate temperature ductility and rupture life.

*MAR-M247 is a trademark of Martin Marietta Industries, Baltimore, MD.

H.Y. BOR, Graduate Ph.D Candidate Student, and C.G. CHAO, Professor, are with the Department of Materials Science and Engineering, National Chiao-Tung University, Taiwan 30050, Republic of China. C.Y. MA, Associate Researcher, is with the Materials R&D Center, Chung-Shan Institute of Science and Technology, Lung Tan, Taiwan 32536, ROC.

Manuscript submitted March 2, 1998.

Table I. Chemical Composition (Wt Pct) of MAR-M247 Superalloys Analyzed by XRF for Major Elements and GDMS for Mg

Heat Number	Co	Cr	Mo	W	Ta	Ti	Al	Hf	Zr	C	Mg (ppm)	O (ppm)	S (ppm)	Ni
EMS-55447	9.0 to 11.0	8.0 to 8.8	0.5 to 0.8	9.5 to 10.5	2.8 to 3.3	0.9 to 1.2	5.3 to 5.7	1.2 to 1.6	0.03 to 0.08	0.13 to 0.17	—	25 max	150 max	bal
1*	10.1	8.32	0.69	9.91	3.16	1.00	5.56	1.51	0.05	0.15	8	6	3	bal
2	10.1	8.20	0.71	9.86	3.17	1.04	5.69	1.37	0.04	0.15	20	8	4	bal
3	10.2	8.24	0.73	9.95	3.11	1.02	5.54	1.31	0.04	0.15	30	7	5	bal
4	10.2	8.21	0.71	9.86	3.09	1.00	5.57	1.31	0.04	0.15	50	9	4	bal
5	10.1	8.14	0.72	9.74	3.00	0.97	5.47	1.29	0.04	0.15	80	5	3	bal

*The Mg content of heat 1 (8 ppm) originated from the raw or crucible materials.

II. EXPERIMENTAL

The MAR-M247 superalloys used in this study were prepared by vacuum induction melting followed by remelting them in a vacuum furnace and then casting them into test bars. The pouring and mold temperatures were 1753 and 1373 K, respectively. Five heats of MAR-M247 superalloys with Mg contents ranging from 20 to 80 ppm were prepared during remelting. After casting, the Mg contents of each heat were analyzed by glow discharge mass spectrometry (GDMS) and the major element compositions were detected by X-ray fluorescence (XRF). The compositions of the parent alloys used in this investigation are given in Table I. The Mg content (8 ppm) of alloy 1 originated from the raw or crucible materials during primary melting. All test bars were subjected to heat treatment under vacuum. Solution treatment was conducted at 1458 K for 2 hours and then argon quenched. Subsequently, the test bars were aged at 1144 K for 20 hours and cooled to room temperature in a furnace.

The microstructure was characterized by optical microscopy, scanning electron microscopy (SEM), and high resolution transmission electron microscopy (HRTEM). The density, area fraction, aspect ratio, and size of various carbide particles for the as-cast samples were measured by using a LECO* 2000 image analyzer. Thirty optical microscope adjoining fields from the polished samples were taken at a magnification of 500 times for each specimen. Segregation of Mg was analyzed by Auger electron spectrometry (AES). In order to minimize specimen contamination or surface gas adsorption, specimens were impacted in the vacuum chamber of the Auger spectroscope at a liquid nitrogen temperature to obtain a fresh fracture surface. In accordance with Engine Material Specification EMS-55447, tensile tests were carried out at 1172 K using an Instron mechanical testing machine. The creep tests were conducted under 1033 K/724 MPa using SATEC M3 creep testers. The gage size of all test bars was 6.3-mm diameter and 26-mm length. The fractograph was examined in a 6400 scanning electron microscope equipped with an energy dispersive spectroscope for microanalysis.

*LECO is a trademark of LECO Corporation, St. Joseph, MI.

III. RESULTS

A. *Microstructure*

Figure 1 illustrates a typical microstructure of a Mg-free MAR-M247 superalloy after the solution and aging heat treatment. In general, it contains (1) the γ matrix phase, (2) γ' precipitates with two distinct sizes ranging from 0.5 to 1.0 and 0.1 to 0.2 μm (Figure 1(a)), (3) a rosette structure of γ-γ' eutectic in the interdendritic region (Figure 1(b)), and (4) scriptlike MC carbides within the grain interior and $M_{23}C_6$ carbides at the grain boundary (Figure 1(c)).

It was observed that the microadditions of Mg did not affect the grain size of the MAR-M247 superalloy. The average grain size obtained in this study is about 2 to 3 mm, as shown in Figure 2. However, the morphology of the scriptlike carbide was significantly changed by the Mg microaddition. For the Mg-free MAR-M247 superalloy, a variety of coarse and scriptlike carbides are present, and the

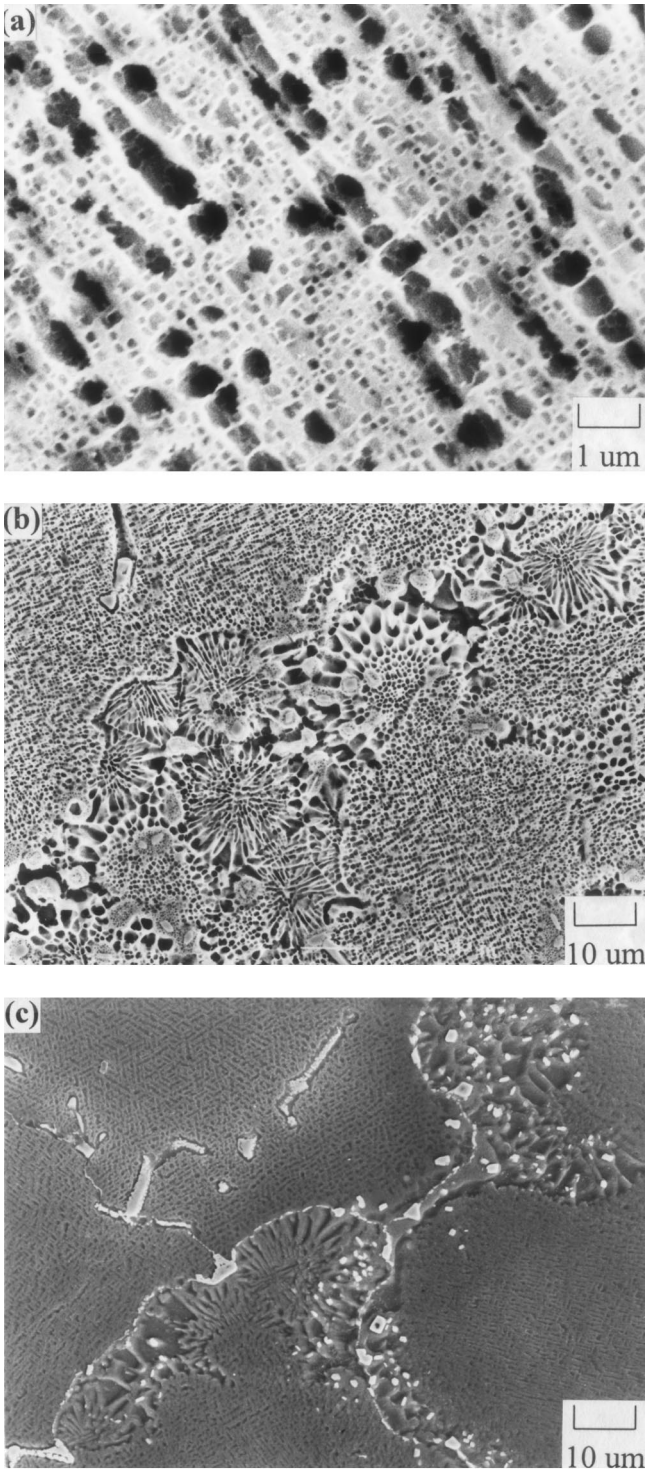

Fig. 1—Microstructures of a Mg-free MAR-M247 superalloy after heat treatment: (*a*) morphology of γ' phase, (*b*) morphology of γ-γ' eutectic structure, and (*c*) MC scriptlike carbides within the grain interior and $M_{23}C_6$ carbides at the grain boundary.

size of these carbides is in excess of 30 μm (Figure 3(a)). When 20 ppm Mg is incorporated, the carbides become finer, although they still exhibit a scriptlike shape (Figure 3(b)). This shape is modified as the Mg contents reach 80 ppm. As can be seen in Figure 3(c), the carbide particles are apparently refined and spheroidized for the MAR-M247 superalloy containing 80 ppm Mg. Obviously, the optimal

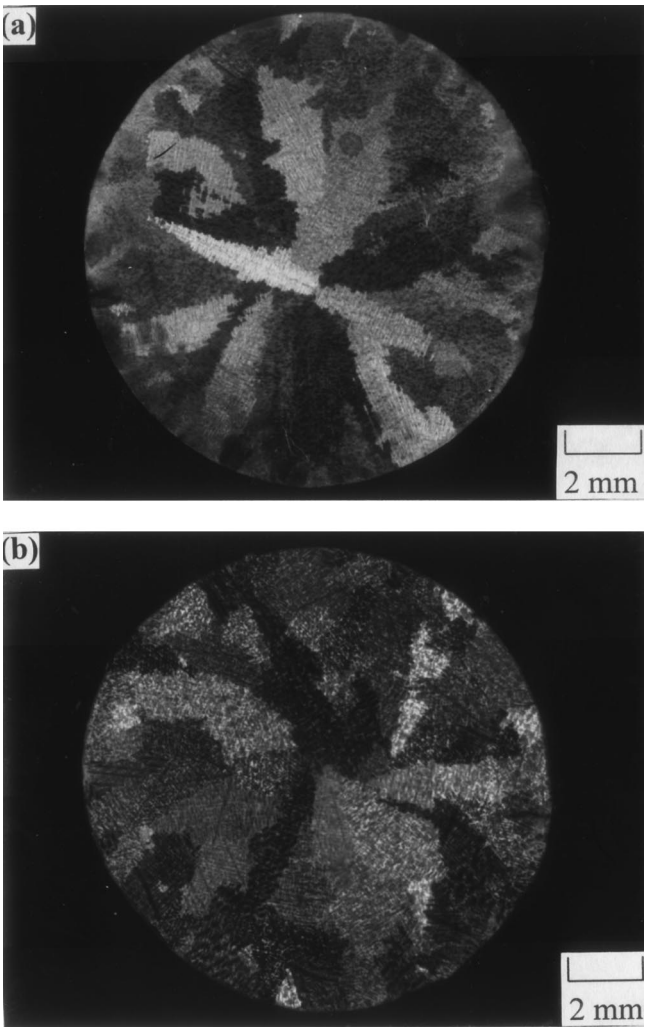

Fig. 2—The grain size of two MAR-M247 superalloys: (*a*) Mg-free and (*b*) 80 ppm Mg.

microaddition of Mg can refine carbide particles or inhibit the precipitation of scriptlike carbides, while the grain size remains unaffected.

B. *Image Analysis Results*

Figure 4 shows the image analysis results of carbides in the MAR-M247 superalloy with various Mg contents. Basically, the area fraction of the carbides (2.2 to 2.5 pct) in MAR-M247 superalloy is not affected by the Mg content, but there are changes in the particle size, aspect ratio, and particle density of the carbides. In Figure 4(b), the carbide particle size decreases with increasing Mg content. The particle size of the carbides in the MAR-M247 superalloy containing 80 ppm Mg is reduced to 3.6 μm, while the carbides in Mg-free alloy have an average size of 5.2 μm. Thus, the elongated or coarse scriptlike carbides are refined due to the microaddition of Mg in the MAR-M247 superalloy.

Figure 4(c) shows the aspect ratio of carbides as a function of Mg content. As the Mg content increases, the aspect ratio decreases. This means that the phenomenon of carbide spheroidization is achieved as a result of the Mg addition. Moreover, the carbide particle density dramatically increases with increasing Mg content, as shown in Figure

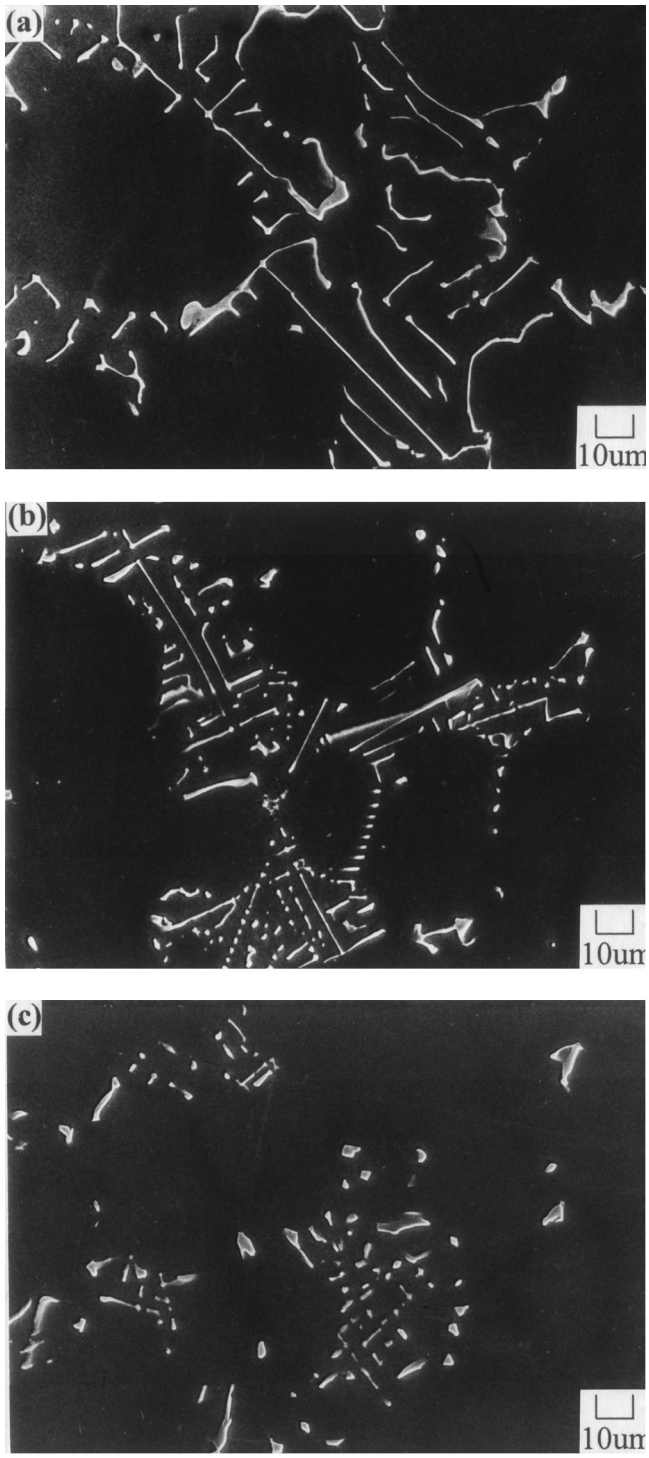

Fig. 3—The morphology of MC carbides in MAR-M247 superalloys with various Mg contents: (*a*) Mg free, (*b*) 20 ppm Mg, and (*c*) 80 ppm Mg.

4(d). This leads to an increase in the total number of carbide particles.

C. *Tensile and Creep Tests*

The tensile properties of MAR-M247 superalloy with various Mg contents tested at 1172 K are given in Table II. Generally, the yield and ultimate strength, which are independent of the Mg content, far exceed the EMS-55447 values. However, the high-temperature elongation remarkably increases by the Mg microaddition. As can be seen in Table II, the elongation of the MAR-M247 superalloy with 80 ppm Mg reaches 14 pct, which is 3 times greater than that of the Mg-free alloy at 1172 K.

According to EMS-55447, the rupture life of the MAR-M247 superalloy must be greater than 23 hours and the elongation is not allowed to be less than 2 pct at 1033 K/724 MPa. For the Mg-free alloy, the elongation can be greater or smaller than the specification value, as given in Table III. However, the rupture elongation is found to be markedly promoted up to 4 pct in the MAR-M247 superalloy containing 20 ppm Mg. It is more obvious that the rupture elongation and life increase with increasing Mg content. Particularly, when the Mg content goes up to 80 ppm, the rupture elongation and life can reach 5.8 pct and 180 hours, respectively. In other words, the rupture life of the MAR-M247 superalloy with 80 ppm Mg is approximately 3 to 5 times greater than that of the Mg-free one. As can be seen in Figure 5, the creep rupture of the Mg-free alloy occurs during the second stage of creep, *i.e.*, without entering the third stage. In contrast, as the alloys containing Mg range from 30 to 80 ppm, the second stage period of creep is effectively prolonged 2 to 3 times. It is noteworthy that the third stage of creep clearly takes place accompanying the plastic strain in these specimens. Apparently, due to the optimal Mg microaddition, both the rupture elongation and the life of the MAR-M247 superalloy are effectively enhanced. In addition, the creep rates of the steady state are also lowered because of the Mg incorporation, as demonstrated in Table III.

D. *Fractographic Observation*

In order to investigate the effect of Mg microaddition on fracture behavior at elevated temperatures, examination of both the fracture surface and the longitudinal section adjacent to the fracture region was made. For a Mg-free specimen crept under 1033 K/724 MPa, a continuous carbide film that was 2 to 3 μm thick is clearly found at the fractured position, as shown in Figure 6(a). It is more evident in Figure 6(b) that a scriptlike carbide is completely pulled out owing to the poor cohesion at the interface. Obviously, the onset of rupture occurs because cracks primarily initiate and propagate along carbide/matrix interfaces or at carbides. These carbides are identified to be TaC or HfC by using SEM/energy dispersive spectroscopy (EDS). For Mg-containing samples, however, the fractography is quite different. As can be seen in Figure 7, most of the cracks are formed along the γ-γ' eutectic rather than at the carbide/matrix interface in a 80 ppm Mg-containing specimen. Observations from the fracture surfaces (Figure 8) show identical evidence; that is, the rupture of Mg-free MAR-M247 occurs mainly along the interface of coarse or scriptlike carbides, while the Mg-containing alloy exhibits a relatively ductile fracture surface.

Moreover, the same results are also obtained in the specimens that were tensile tested at 1172 K. Figure 9 shows two distinct SEM fractographs, revealing the significant changes in carbide morphology and fractography owing to the Mg addition. In Figure 10, the continuous MC carbide films distributed on the fractured surface, and the interfacial decohesion of carbide/matrix is clearly observed from the longitudinal fracture portion of a Mg-free MAR-M247 su-

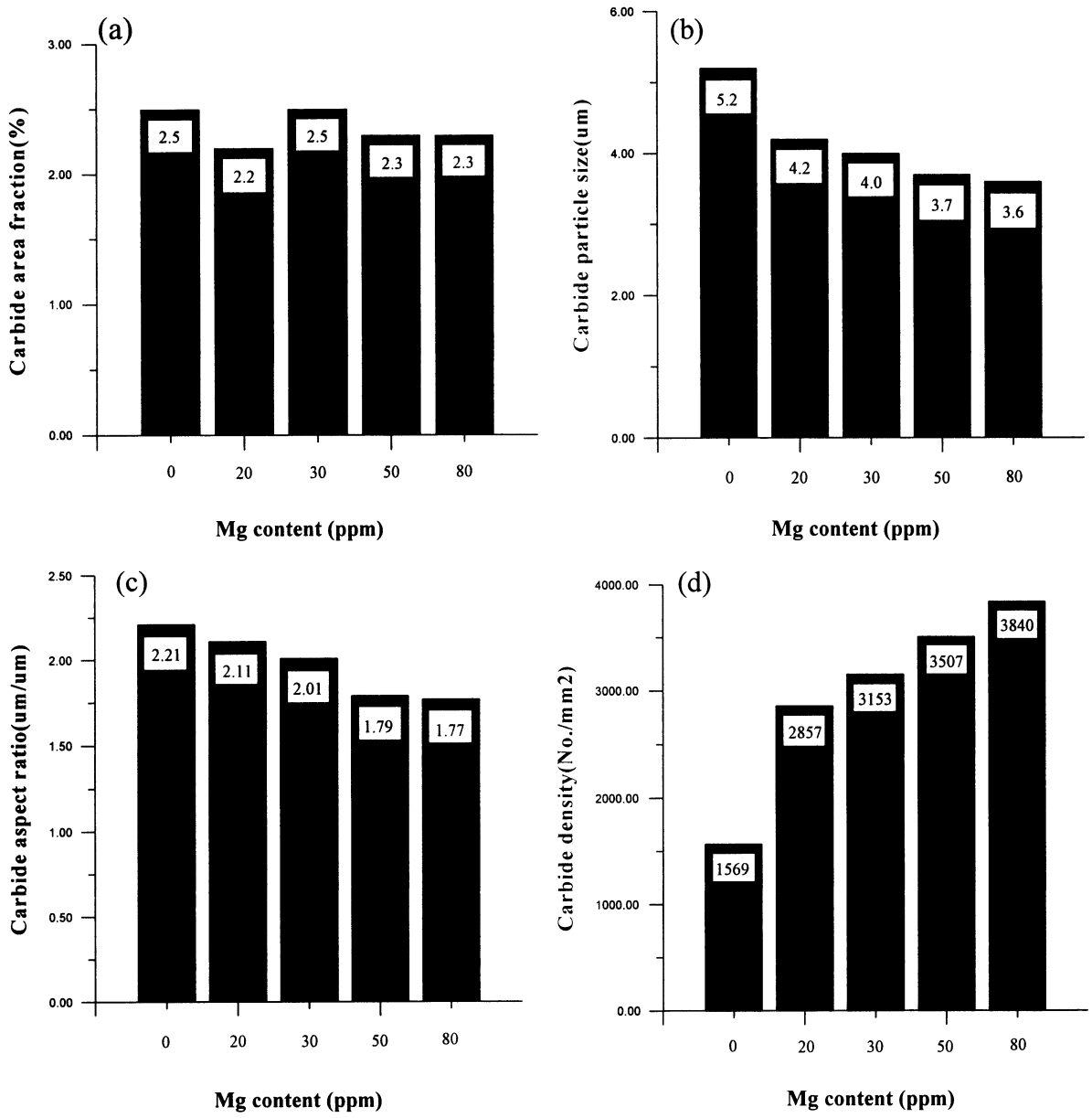

Fig. 4—Image analysis results of carbide characteristics in MAR-M247 superalloys with various Mg contents: (*a*) area fraction, (*b*) particle size, (*c*) aspect ratio, and (*d*) particle density.

Table II. Tensile Test Results of MAR-M247 Superalloys with Various Mg Contents at 1172 K

Mg Content	YS (MPa)	UTS (MPa)	Elongation (Pct)
EMS 55447 (without Mg)	414	690	4
Without Mg	576 to 676	788 to 794	3.6 to 4.7
20 ppm Mg	652 to 653	803 to 812	5.1 to 7.6
30 ppm Mg	633 to 658	840 to 851	5.5 to 7.6
50 ppm Mg	584 to 606	808 to 810	8.9 to 9.0
80 ppm Mg	610 to 617	803 to 809	13.7 to 14.0

Table III. Creep Test Results of MAR-M247 Superalloys with Various Mg Contents under the Condition of 1033 K/ 724 MPa

Mg Contents	Creep Life (h)	Elongation (Pct)	Creep Rate (s^{-1})
EMS 55447 (without Mg)	>23	>2	—
Without Mg	28 to 63	1.9 to 2.4	7.4×10^{-8}
20 ppm Mg	55 to 87	3.0 to 4.2	7.3×10^{-8}
30 ppm Mg	140 to 156	3.7 to 3.9	3.9×10^{-8}
50 ppm Mg	178 to 180	4.4 to 4.5	3.7×10^{-8}
80 ppm Mg	170 to 184	5.6 to 5.8	3.9×10^{-8}

peralloy. Conversely, the ductile fracture along the γ-γ' eutectic, as indicated in Figure 11, is demonstrated in a 80 ppm Mg alloy.

Overall, the crack initiation sites are basically consistent with the observed crack path along the fracture surface. In Mg-free alloys, some secondary cracks located at the carbide/matrix interface are observed along the gage section of creep rupture and tensile fracture specimens (Figures 6(b) and 10(b)).

E. *Analysis of Mg Segregation*

In order to explore the effect of Mg microadditions on carbide characteristics, AES was employed for interfacial segregation analysis. Standard AES samples without and with 80 ppm Mg were prepared and subjected to liquid nitrogen for 4 hours before impact tested. Figure 12(a) shows a secondary electron image of the fractured surface of a 80 ppm specimen, where two typically distinct regions are selected and marked, *i.e.*, ductile region (area 1) and cleavage surface (area 2). Figures 12(b) and (c) are the corresponding Auger spectra, revealing the regions of the matrix (including γ') and a MC carbide, respectively. Apparently, no or limited Mg is detected in the matrix (Figure 12(b)) and within the carbide interior (Figure 12(c)). On closer observation, several pull-out sites of carbide are found, as shown in Figure 13(a). The pulled-out carbide was identified to be a MC type when the corresponding fractured surface of the opposite side was determined by EDS. For the site where carbide decohesion occurred, the Mg peak in the spectrum (magnified in the inset) depicts Mg enrichment at the carbide/matrix interface (Figure 13(b)). Since the sensitivity of AES is 1000 ppm, and Mg was detected at the matrix/carbide interface (as compared with the average content of 80 ppm analyzed with GDMS), these results indicate that Mg segregation has occurred. At the same region, comparatively high oxygen and sulfur levels are also illustrated by the greater O and S peaks (Figure 13(b)). However, little evidence of Mg segregation was found in any Mg-free specimens by using the same examination method mentioned previously. In addition, the phenomenon of Mg segregation to GB was not found in this study, owing to a relatively large grain size (2 to 3 mm)

IV. DISCUSSION

A. *Mechanisms for Mg Segregation*

According to the present AES results, Mg significantly segregates to carbide/matrix interfaces, in particular, to MC carbides with a concentration (at least 1000 ppm) much greater than the average level (80 ppm). The same result has been reported in a directionally solidified Ni-based superalloy and some cast superalloys.[28,34] Concerning the mechanism for Mg segregation, Ge *et al.* have proposed that the Mg segregation is due to the uphill diffusion of Mg to the Ni-enriched interfacial liquid surrounding the growing carbide particles, which arises from the negative excess Gibbs free energy change for a Ni-Mg liquid solution.[34] In other words, Mg accumulation adjacent to the carbides is a result of diffusional transport to the interfacial region in the liquid, and that is a typical interfacial enrichment mechanism. In addition, Zhu *et al.*[30] have reported that Mg is readily concentrated around the GB and at the incoherent interface between a carbide and the matrix to form a layer of Ni_2Mg Laves phase with a thickness of 20 nm. However, the Lave phase of Ni_2Mg was not found in the Mg-containing MAR-M247 superalloy by using HRTEM in this investigation.

Another mechanism is based on the premise that the Mg binds with harmful elements at the interface. Since Mg has a limited solubility in the matrix and would be inclined to accumulate at a carbide/matrix interface, it operates by neutralizing embrittling impurities such as oxygen or sulfur. This mechanism is basically consistent with the present AES results (Figure 13). Some investigations[19,26] reported that a low melting point, brittle compound of MgS might form as a result of Mg segregation to interfaces. However, the MgS phase was not observed at either the matrix/carbide interface or GB by using HRTEM. In case the MgS phase was formed, this would promote the occurrence of cracking at the interface and impair the ductility, which is contrary to the present test results.

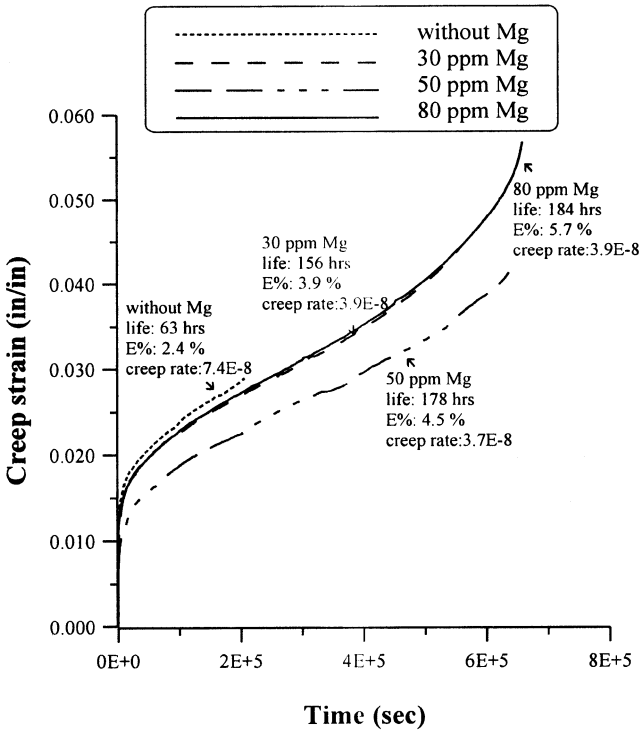

Fig. 5—Creep curves of MAR-M247 superalloys with various Mg contents tested under the condition of 1033 K/724 MPa.

Other investigations[32] reported that Mg might also segregate to γ' and the γ-γ' interface, which has a semicoherent interface with the matrix. From the present results, evidence of Mg segregation to γ' and γ-γ'/matrix interfaces was not obtained by using AES and HRTEM/EDS. It is believed that the tendency for Mg segregation to the carbide/matrix interface is much more likely than to the γ' and γ-γ'/matrix interfaces, since the interface between MC carbide/matrix, based on the HRTEM analysis and the thermodynamics of interfacial segregation, is incoherent.

B. *Influence of Mg Segregation on Carbide Morphology*

According to the present results, the coarse or scriptlike MC carbides were formed in a Mg-free MAR-M247 superalloy, while an optimal addition of Mg significantly changed the carbide morphology. Bhambri *et al.* proposed that the morphology MC carbide is faceted and octahedral with {111} faces and ⟨100⟩ rapid growth direction during solidification.[37] Under this circumstance, the elongated or scriptlike morphology is formed. As has been mentioned previously, Mg is a surface-active element and has a high propensity for segregating to the carbide/matrix interface, causing a Mg-enriched layer to develop surrounding the

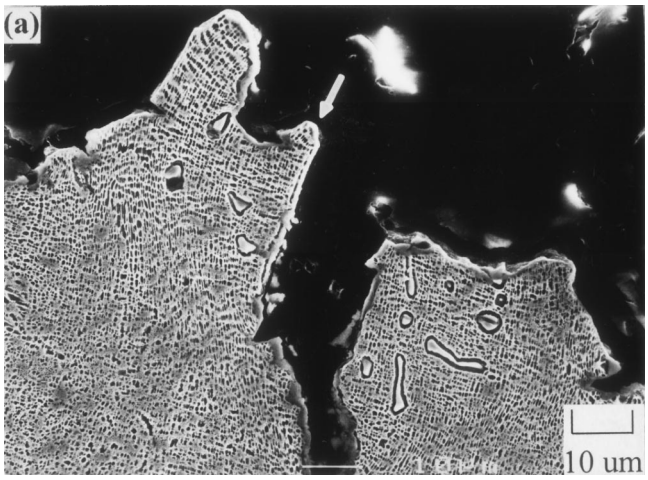

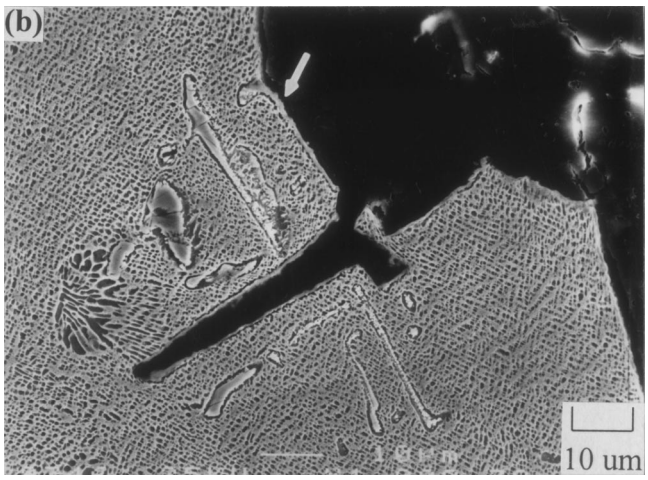

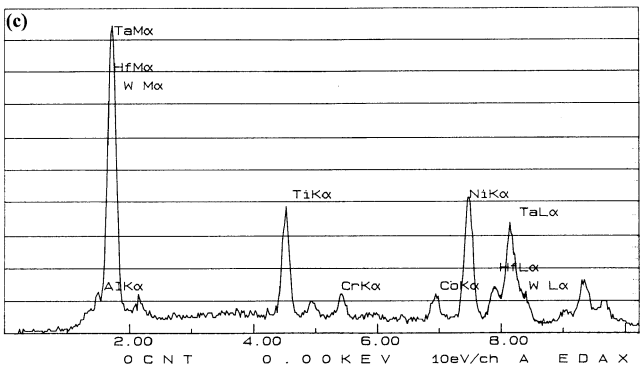

Fig. 6—Longitudinal section of a crept MAR-M247 superalloy without Mg tested under 1033 K/724 MPa: (*a*) and (*b*) fractographs and (*c*) EDS measurement results at the fractured position.

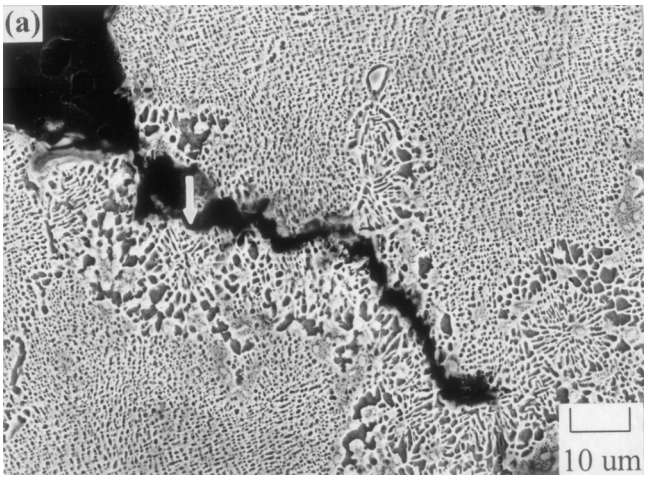

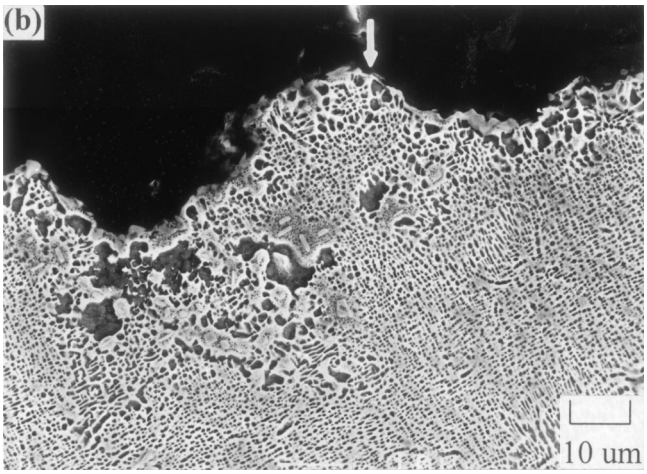

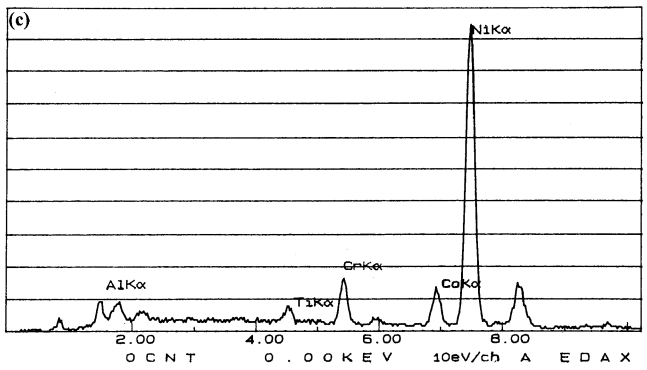

Fig. 7—Longitudinal section of a crept MAR-M247 superalloy containing 80 ppm Mg tested under 1033 K/724 MPa: (*a*) and (*b*) fractographs and (*c*) EDS measurement results at the fractured position.

carbides.[34] This layer might influence the transport of carbon and the carbide forming elements, such as Hf, Ta, or W. It could result in the isotropic growth of carbides during solidification and eventually lead to the refinement and spheroidization of MC carbides in the MAR-M247 superalloy.

C. *Influence of Mg Microaddition on Creep Behavior*

Based on the creep curves in Figure 5, crack initiation and propagation during creep are clearly retarded in Mg-containing alloys, and consequently, the rupture life is substantially prolonged. According to the creep deformation map of a MAR-M247 related superalloy,[38] the creep mechanism under the condition of 1033 K/724 MPa should be dislocation glide; that is, the creep behavior is dominated by the interaction between dislocations and obstacles such as precipitates or carbides. From fractographic observations, the onset of fracture mainly occurs at the interface of the carbide/matrix in the Mg-free alloy. Also, Baldan[39] pointed out that the size of the carbide particles is dominant in determining the creep rupture ductility, and a fine dis-

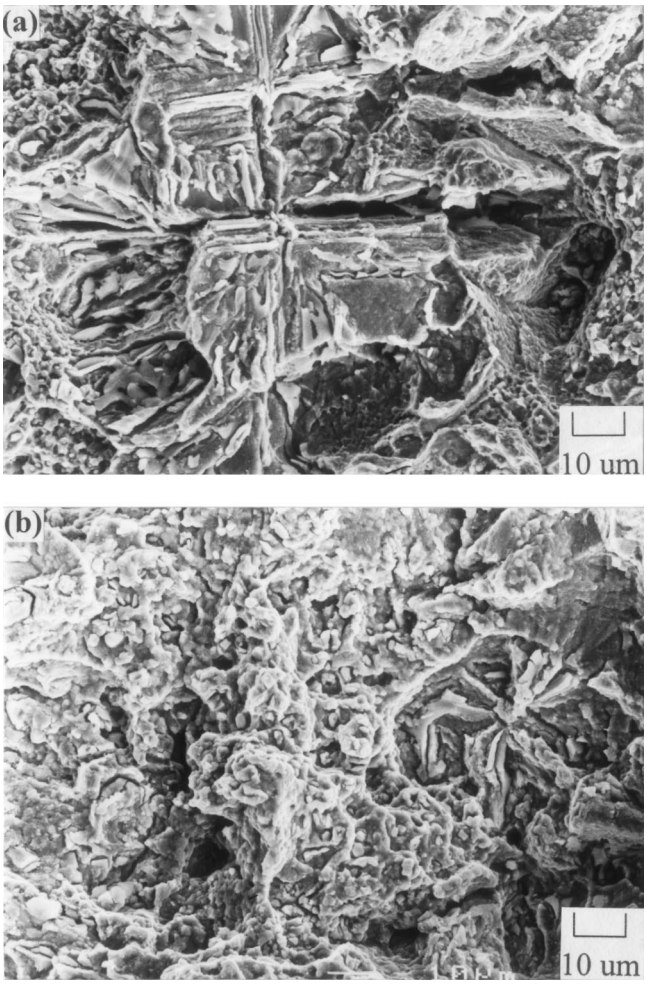

Fig. 8—Fractographs of MAR-M247 superalloys under 1033 K/724 MPa: (*a*) Mg free and (*b*) 80 ppm Mg.

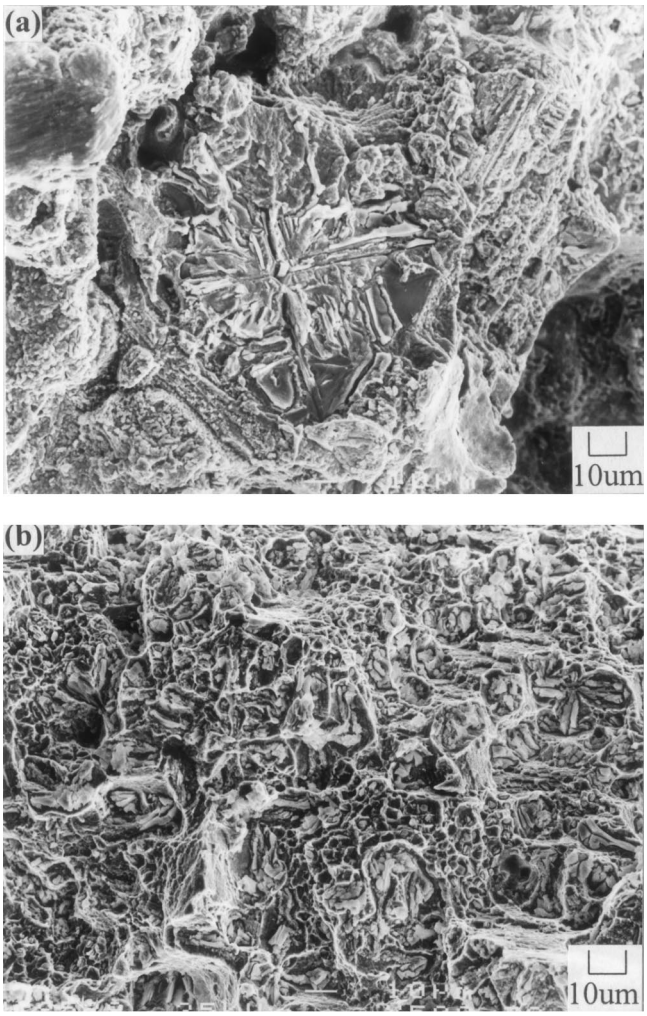

Fig. 9—Fractographs of MAR-M247 superalloys tensile tested at 1172 K: (*a*) Mg free and (*b*) 80 ppm

persion leads to higher creep ductility. According to some investigations on Mg-addition effect,[19,30,34] furthermore, the spheroidized carbides should change the stress state around carbides and reduce lowering the occurrence of crack formation. Therefore, the beneficial effect of Mg is on the change in MC carbide morphology and possibly on affecting the cohesive energy of carbide/matrix interface in the present study.

In research on the creep behavior in Mg microalloyed wrought superalloys, Ma *et al.*[19] reported that Mg could purify the GB and increase the GB cohesive energy by binding the detrimental elements. This causes an enhancement of creep behavior of superalloy. In the present study, the grain size is relatively large. The rupture mode, which is irrelevant to the Mg addition, is a typical mixture of intergranular and transgranular in all rupture specimens. This means that the effect of GB purification might not be a dominant mechanism responsible for the enhancement of creep behavior due to Mg microalloying in the current MAR-M247 superalloy.

Further, Ma *et al.*[32] demonstrated that the solid solution strengthening effect of Mg in carbides, γ', and γ-γ' might contribute to the enhancement of the mechanical behavior in Ni-based superalloys. In the present work, however, no or limited Mg was detected in any of these phases by using AES. In fact, γ' and carbide forming elements such as Ni, Cr, Al, Ti, W, Mo, Hf, and Ta have much smaller atomic radii (0.125 to 0.145 nm) than that of Mg (0.160 nm). When Mg atoms dissolve into γ' or carbides, the lattices of these phases will be severely distorted and will cause an increase in total energy. This effect is, obviously, unfavorable from the viewpoint of thermodynamics.

The present results also show a trend of a decrease in the steady-state creep rate in Mg-containing alloys. The same results were reported by Ma *et al.*,[19,26] who pointed out that the microaddition of Mg in a Ni-based superalloy will increase the vacancy formation energy (Qv) and decrease the vacancy concentration under the conditions of high temperature and low stress, *i.e.*, in the range of low strain rates. These conditions will lower the velocity of dislocation climb through the γ' and also decrease the steady-state creep rate in the Mg-containing alloy.[19,26] As has been mentioned earlier, however, the mechanism of dislocation glide should be the prevailing mechanism at moderate temperature and high stress (*i.e.*, high strain rate) in this study. On this basis, the mechanism of vacancy concentration decrease might not be directly associated with the decrease of steady-state creep rate achieved here. Hence, more relevant work is needed to explain this phenomenon.

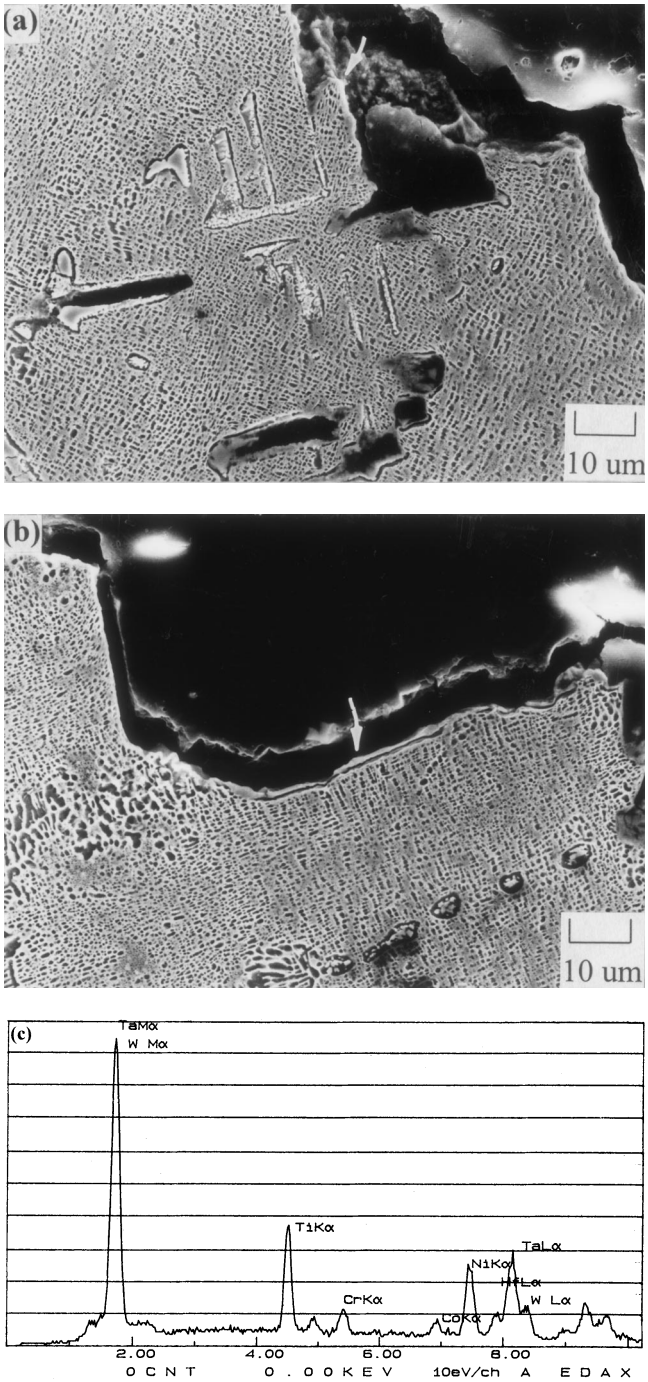

Fig. 10—Longitudinal section of a fractured specimen without Mg addition tensile tested at 1172 K. (*a*) and (*b*) fractographs and (*c*) EDS measurement results at the fractured position.

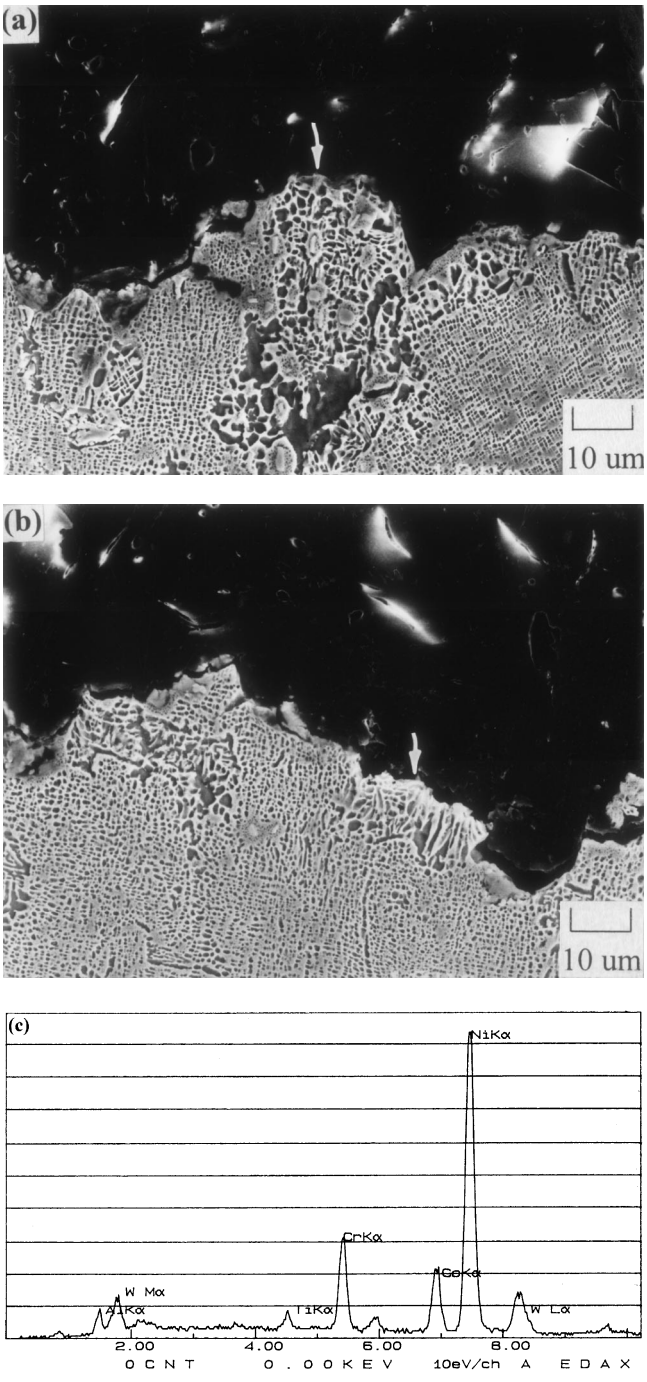

Fig. 11—Longitudinal section of a fractured specimen containing 80 ppm Mg tensile tested at 1172 K: (*a*) and (*b*) fractographs and (*c*) EDS measurement results at the fractured position.

D. *Influence of Mg Microaddition on Fracture Mechanism*

In the late 1970s, alloy designers added Hf to Ni-based superalloys for the purpose of producing the γ-γ' eutectic and increasing the GB toughness;[1,2,7] however, MAR-M247 remained brittle at elevated temperatures.[5,6] From the fractographic observations, crack initiation preferentially occurs at the MC carbide/matrix interface in the Mg-free MAR-M247 superalloy at elevated temperatures. The same evidence has been demonstrated by Kaufman,[6] who proved that scriptlike MC carbides were extremely brittle and could act as crack initiation sites or crack propagation paths. By adding small amounts of Mg, these carbides are apparently refined and spheroidized. From some previous results in wrought superalloys,[19,22,30] Mg microadditions may cause a change in interfacial energy and improve the cohesion between the carbide and the matrix. This leads to a change of stress state in front of the carbides. In the present study, Mg was detected to segregate to the carbide/matrix interface and the coarse carbides were refined and spheroidized. Under this circumstance, crack initiation

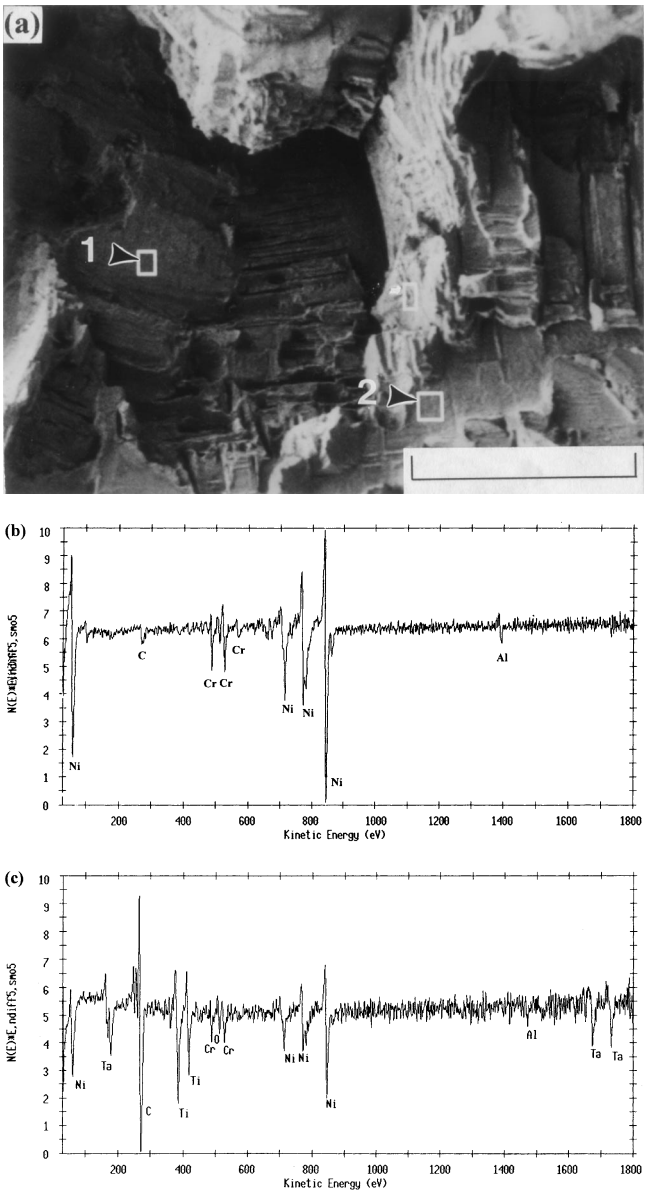

Fig. 12—(*a*) The secondary electron image of a fractured surface, (*b*) Auger spectrum analyzed from area 1 in Fig. 15(a), and (*c*) Auger spectrum analyzed from area 2 in Fig. 15(a).

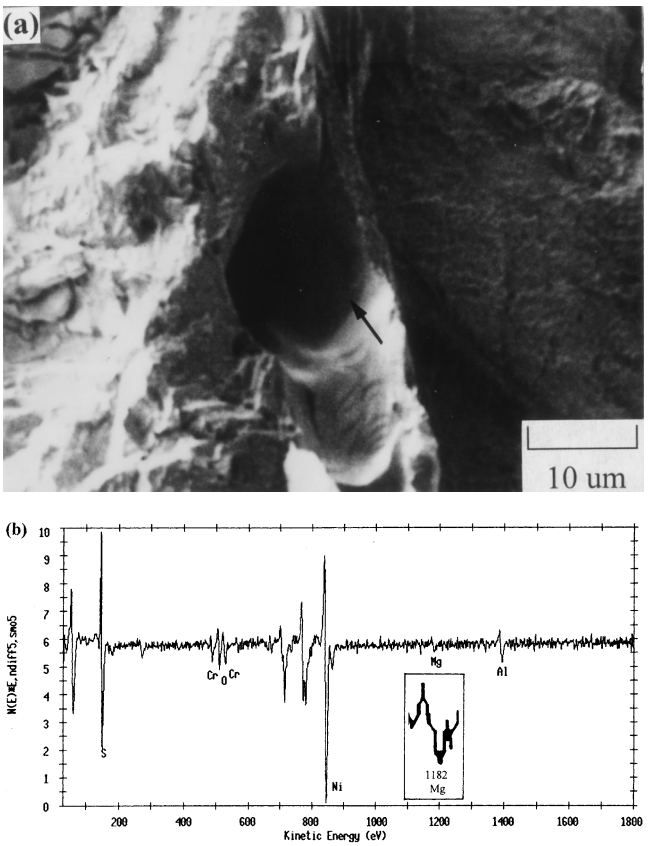

Fig. 13—(*a*) The secondary electron image of a fractured surface, showing a pulled-out and decohesion site of a MC carbide; and (*b*) Auger spectrum analyzed from the MC carbide/matrix interface.

is observed to occur at the γ-γ' eutectic, a region having superior ductility.[40] Consequently, a transition of fracture mode from the carbide/matrix interface to the γ-γ' eutectic region occurs. The crack initiation and propagation are substantially retarded, and the rupture life and elongation are improved. Finally, it should be emphasized here that wedge and cavitation crack modes reported in the literature[19] are not applicable in this study, since relatively large grain sizes were achieved in the present investigation.

V. CONCLUSIONS

The effects of Mg microaddition on the mechanical behavior and fracture mechanism in MAR-M247 superalloys can be summarized from the present investigation results as follows.

1. The Mg microaddition inhibits the formation of scriptlike MC carbides and causes the refinement and spheroidization of MC carbides, while the grain size remains unaffected.
2. The elongation of Mg-containing MAR-M247 superalloy tested at 1172 K is significantly increased. When the Mg content is increased up to 80 ppm, the 1172 K elongation dramatically reaches 14 pct.
3. The microaddition of 30 to 80 ppm Mg in the MAR-M247 superalloy effectively prolongs rupture life and elongation. In particular, the rupture life and elongation of the MAR-M247 superalloy with 80 ppm Mg is significantly improved up to 3 to 5 times that of the Mg-free alloy under the creep condition of 1033 K/724 MPa.
4. The AES results indicate that Mg segregates to the carbide/matrix interface and there is little evidence of Mg detected in any other phases. Thus, the beneficial effect of Mg is apparently on the change in carbide morphology and possibly on the affect of the cohesive energy of the carbide/matrix interface.
5. The fracture mainly initiates and propagates along the interface of the scriptlike carbide and matrix in Mg-free MAR-M247 superalloy during the 1172 K tensile and 1033 K/724 MPa creep tests. In contrast, fracture occurs along the γ-γ' eutectic in the Mg-containing alloy, causing a retardation in crack initiation and improving the rupture ductility and life at elevated temperatures.

ACKNOWLEDGMENTS

This work was conducted under the National Science Council of the Republic of China, Research Project No.

NSC 86-2623-D-009-006. The authors thank Dr. J.Y. Wang and Mr. S.C. Yang for their help with the HRTEM observation and mechanical property evaluation. The equipment support of processing from Mr. J.S. Chen, Dr. T.S. Lee, and Dr. Y.L. Lin is thankfully acknowledged.

REFERENCES

1. J.E. Doherty, B.H. Kear, and A.F. Giamei: *J. Met.*, 1971, vol. 23 (11), pp. 59-62.
2. D.N. Duhi and C.P. Sullivan: *J. Met.*, 1971, vol. 23 (7), pp. 38-40.
3. M.V. Nathal, R.D. Maier, and L.J. Ebert: *Metall. Trans. A*, 1982, vol. 13A, pp. 1767-74.
4. M.V. Nathal, R.D. Maier, and L.J. Ebert: *Metall. Trans. A*, 1982, vol. 13A, pp. 1775-83.
5. ''Castings, Investment, MAR-M247,'' Allied-Signal Aerospace Company: Engine Materials Specification 55447, Allied-Signal Aerospace Company, P.O. Box 52181, Phoenix, AZ, 1988.
6. M. Kaufman: *Proc. Superalloys 1984*, M. Gell, C.S. Kortovich, R.H. Bricknell, W.B. Kent, and J.F. Radavich, eds., AIME, Warrendale, PA, 1984, pp. 43-52.
7. P.S. Kotval, J.D. Venables, and R.W. Calder: *Metall. Trans.*, 1972, vol. 3, pp. 453-58.
8. T.B. Gibbons and B.E. Hopkins: *J. Met. Sci.*, 1971, vol. 5, pp. 233-40.
9. G.R. Leverant and M. Gell: *Trans. TMS-AIME*, 1969, vol. 245, pp. 1167-73.
10. D.R. Muzyka and C.R. Whitney: ''Process for Making Nickel Base Precipitation Hardenable Alloys,'' U.S. Patent 3,575,734, Apr. 20, 1971.
11. W. Garcia and J.A. Butzer: ''Nickel-Base Casting Superalloys,'' U.S. Patent 4,140,555, Feb. 20, 1979.
12. T. Handa and Kanagawa: ''Low Thermal Expansion Casting Alloy Having Excellent Machinability,'' U.S. Patent 4,904,447, Feb. 27, 1990.
13. J.J. deBarbadillo: *Proc. 3rd Int. Symp., 1976, Superalloys Metallurgy and Manufacture*, B.H. Kear, D.R. Muzyka, J.K. Tien, and S.T. Wlodek, eds., Claitor's Publishing Division, Baton Rouge, LA 70821, 1976, pp. 95-107.
14. G.Z. Lu, B.K. Zhao, S.H. Li, and G.P. Zhao: *J. Iron Steel Res.*, 1992, vol. 4 (2), pp. 63-67.
15. J. Schramm: U.S. Patent No. 3,512,963, May 19, 1970.
16. L.M. Rober and N.C. Charlotte: U.S. Patent No. 4,376,650, March 15, 1983.
17. L.M. Rober and N.C. Charlotte: U.S. Patent No. 4,456,481, June 26, 1984.
18. J.M. Moyer: *Proc. Superalloys 1984*, M. Gell, C.S. Kortovich, R.H. Bricknell, W.B. Kent, and J.F. Radavich, eds., AIME, Warrendale, PA, 1984, pp. 443-54.
19. P. Ma, Y. Yuan, and Z.Y. Zhong: *Proc. Superalloys 1988*, S. Reichman, D.N. Duhl, G. Maurer, S. Antolovich, and C. Lund, eds., AIME, Warrendale, PA, 1988, pp. 625-33.
20. X.H. Xie, Z.H. Xu, B. Qu, and G.L. Chen: *Proc. Superalloys 1988*, S. Reichman, D.N. Duhl, G. Maurer, S. Antolovich, and C. Lund, eds., AIME, Warrendale, PA, 1988, pp. 635-42.
21. Y.Q. Li, C.M. Sun, J.Y. Liu, and G.L. Chen: *High Temp. Technol.*, 1987, vol. 5 (4), pp. 201-04.
22. G.L. Chen, T.H. Zhang, and W.Y. Yang: *High Temp. Technol.*, 1988, vol. 6 (3), pp. 149-52.
23. Y.Q. Li and Y.H. Gong: *J. Mater. Sci.*, 1992, vol. 27, pp. 6641-45.
24. G.S. Chyernyak, A.V. Smirnova, and S.B. Maslenkov: *Metall. (Metalli.) SSSR*, 1973, No. 1 pp. 98-104.
25. V.V. Topilin: *Steel (Stal)*, 1978, No. 11 pp. 643-46.
26. P. Ma, Y. Yuan, and Z. Zhong: *Acta Metall. Sinica*, 1989, vol. 25 (6) pp. A449-A453.
27. X. Xie, K. Ni, Z. Xu, G. Ling, and N. Wang: *Mech. Behav. Mater.*, 1991, vol. 4, pp. 613-18.
28. P. Ma and J. Zhu: *Metallography*, 1986, vol. 19, pp. 115-18.
29. Q. Zhu, D. Wang, Q.L. Cheng, J. Fu, Z. Xu, and Q. Qiao: *J. Beijing Univ. Iron Steel Technol.*, 1988, vol. 10 (1), pp. 12-17.
30. J. Zhu, Z.Y. Cheng, and H.Q. Ye: *Scripta Metall.*, 1989, vol. 23, pp. 1537-42.
31. Q. Zhu, D. Wang, H. Ge, and G. Chen: *Acta Metall. Sinica*, 1989, vol. 25 (3), pp. A185-A89.
32. P. Ma, J. Zhuang, J. Yang, and L. Gao: *Acta Metall. Sinica*, 1987, vol. 23 (3), pp. A195-A99.
33. G.L. Chen, D. Wang, Z. Xu, J. Fu, K. Ni, and X. Xie: *Proc. Superalloys 1984*, M. Gell, C.S. Kortovich, R.H. Bricknell, W.B. Kent, and J.F. Radavich, eds., AIME, Warrendale, PA, 1984, pp. 611-20.
34. H.L. Ge, W.V. Youdelis, G.L. Chen, and Q. Zhu: *Mater. Sci. Technol.*, 1989, vol. 5, pp. 985-90.
35. G. Chen, Q. Zhu, D. Wang, and X. Xie: *Superalloy 718*, E.A. Loria, ed., TMS, Warrendale, PA, 1989, pp. 545-51.
36. H.Y. Bor, C.G. Chao, and C.Y. Ma: *Scripta Mater.*, 1998, vol. 38 (2), pp. 329-35.
37. A.K. Bhambri and T.Z. Kattamis: *Metall. Trans. B*, 1975, vol. 6B, pp. 523-37.
38. C.T. Sims, N.S. Stoloff, and W.C. Hagel: *Superalloy II*, John Wiley & Sons, New York, NY, 1987, pp. 39-40.
39. A. Baldan: *Z. Metallkd.*, 1992, vol. 83 (10), pp. 750-57.
40. K.L. Gasko, G.M. Janowski, and B.J. Pletka: *Mater. Sci. Eng.*, 1988, vol. A104, pp. 1-8.